J Appl Electrochem (2014) 44:1205–1218
DOI 10.1007/s10800-014-0737-4

RESEARCH ARTICLE

Effects of anode orientation and flow channel design on performance of refuelable zinc-air fuel cells

Chanipa Jiratchayamaethasakul · Nalinee Srijaroenpramong · Thanadon Bunyangyuen · Wichaya Arpavate · Nutthapon Wongyao · Apichai Therdthianwong · Supaporn Therdthianwong

Received: 1 May 2014 / Accepted: 18 August 2014 / Published online: 26 August 2014

Abstract The effects of anode orientation (whether an anode is located above or under a cathode) and flow channel design (parallel or serpentine flow channel) on the performance of refuelable zinc-air fuel cells (RZAFC) continuously fed with KOH electrolyte were investigated. The performance test was conducted at different electrolyte flow rates of 2, 4, and 6 ml h^{-1}. A polarization test of the cell was conducted at the initial stage of operation, followed by a long-term current discharge test in potentiostatic mode. The spent zinc powders were characterized by a scanning electron microscope and X-ray diffraction. The experimental results revealed that the anode-bottom orientation in the cell performed much better than the anode-top orientation with 11.4 times higher zinc utilization. The performance reduction of the anode-top orientation cell was caused by the cathode overpotential, due to the flooding of the cathode by water crossover from the anode, which was induced by the gravity force. For the flow channel design effects, there was an optimum electrolyte flow rate, to yield a maximum current discharge capacity, of 4 ml h^{-1} in this study. At this optimum flow rate, the total charge per gram of zinc delivered from the anode serpentine cell was 1.75 times higher than that from the anode-parallel one.

Keywords Refuelable zinc-air fuel cell (RZAFC) · Flow electrolyte · Anode orientation · Parallel flow channel · Serpentine flow channel

C. Jiratchayamaethasakul · N. Srijaroenpramong · T. Bunyangyuen · W. Arpavate · S. Therdthianwong (✉)
Department of Chemical Engineering, Faculty of Engineering, King Mongkut's University of Technology Thonburi, 126 Pracha-Uthit Rd., Bang Mod, Thung Khru, Bangkok 10140, Thailand
e-mail: supaporn.the@kmutt.ac.th

N. Wongyao · A. Therdthianwong
Fuel Cells and Hydrogen Research and Engineering Center, Clean Energy System Group, PDTI, King Mongkut's University of Technology Thonburi, 126 Pracha-Uthit Rd., Bang Mod, Thung Khru, Bangkok 10140, Thailand

1 Introduction

High energy density is an extreme requirement for mobile power sources. Although hydrogen fuel cell technology has been developed, energy density of hydrogen fuel at standard temperature and pressure is about 2,500 times less than that of zinc fuel [1]. In addition, zinc handling is much simple than that of hydrogen and safer for users [2, 3]. This makes zinc uniquely suitable for mobile power sources and zinc-air fuel cell is suggested as a possible power source for electric vehicles [4, 5]. Zinc-air batteries can be divided into three main types: primary, secondary, and mechanically rechargeable or refuelable cells [6–8]. Based on the refuelable cells design, the use of the zinc-air system for electric vehicles has high potential and the lifetime of such a cell was limited only by the air cathode, since the utilized zinc and electrolyte can be replaced [1].

Refuelable zinc-air fuel cells (RZAFC) can be designed using the concept of plate-and-frame filter presses. This type of design consists of anode plates and cathode frames assembled alternatively with a membrane separator over each side of the plate. The zinc slurry is fed into the plate, which have channels cut in them so that zinc slurry can flow through and fill the flow channel. The flow direction of zinc slurry is controlled by the design of the flow channel pattern.

The pumping of zinc slurry proceeds until the flow channels are completely filled with zinc solid. When the cells are completely discharged, the anode plates and cathode frames are separated and the utilized zinc powders are removed. Then the cell is reassembled and the cycle is repeated. Although, the above cell design is operated in a batch process, it can be flexible to work in continuous mode if zinc slurry is continually supplied to the cell.

For proton exchange membrane fuel cells design, fuel and oxidant are continuously supplied to the cell via the flow channel. Originally, the design of the flow structure was a single-chamber flow structure (or single compartment). Unfortunately, this single-chamber design led to poor cell performance due to poor reactant distribution. Later, intricate flow structure containing many small flow channels was designed. This flow structure provides uniform reactant distribution, resulting in better cell performance. Among these flow structures, the parallel and serpentine patterns are most generally employed in membrane-based fuel cells [9]. One of the advantages of the parallel pattern is the low overall pressure drop. However, non-uniform flow distribution may occur if the width of the flow field is too large. The serpentine patterns could remove reaction products and handle two-phase mass transport, but may cause a high pressure drop when the length of the flow field is relatively long.

These flow field designs are applied to not only a fuel gas, but also to a liquid phase fuel. The effect of anode flow field design on the performance of liquid-fed direct methanol fuel cells (DMFC) has been studied by many researchers [10, 11]. For DMFCs, it has been shown that the cell orientation had a significant effect on the cell's performance [10]. The experiments with the serpentine flow field have shown that cell orientation could influence the two-phase flow behavior of gaseous CO_2 product and methanol feed solution leading to cell performance determination, especially at low methanol flow rates. Two-phase flow is expected to take place in anode zinc-air fuel cells (ZAFC) because of the formation of H_2 gas according to the side reactions as indicated below [1, 12]:

$$Zn + 2\ H_2O \rightarrow Zn(OH)_2 + H_2 \quad (1)$$

$$Zn + Zn(OH)_2 \rightarrow 2\ ZnO + H_2 \quad (2)$$

In this research study, refuelable zinc-air fuel cells in a plate-and-frame filter manner were constructed. The effects of flow field pattern and the orientation of the anode plate on the performance of RZAFCs fed continuously with KOH electrolyte at different flow rates were investigated. The orientations of the anode plate were achieved by placing it horizontally above or under the cathode plate.

2 Experimental procedures

2.1 Materials and cell preparation

The anode of RZAFC mainly consists of zinc powder having particle size distribution of 53–150 microns and was filled in flow channels of the anode plate. The cathode catalyst material was a mixture of Vulcan XC 72 carbon powder, manganese dioxide (MnO_2) as catalyst, and Nafion® solution as a binder at weight ratios of 1.3:1.3:1.0, in a deionized water-isopropanol solvent mixture. This ink was then painted on a stainless steel mesh number 300 at a loading of 3.5 mg of MnO_2 cm^{-2} to form a cathode. The membrane separator used was Celgard® 5550 polypropylene and 8.0 M KOH electrolyte was employed in this study.

The cell was constructed by assembling the anode, membrane separator and cathode with the air electrode as the cathode and the zinc powder as the anode. At the anode side, the anode flow channel and the current collector were installed. The cathode side consists of the coated stainless mesh and a current collector having many small holes to allow free convection of inlet air. To assemble a cell, two sheets of polymethyl methacrylate (PMMA) were used as the end plates.

During cell operation, potassium hydroxide electrolyte was supplied into the cell using a peristaltic pump. The zinc-air fuel cell performance test was carried out for 250 min using two types of anode configurations: square and serpentine, as shown in Fig. 1. Both flow channels have the same cross-sectional area of 14.1 cm^2 and the same depth of 0.3 cm. Initially, gelled zinc slurry was transferred by a peristaltic pump into the anode flow channel until the channel was full.

2.2 Flow channel design and anode orientation

The parallel and the serpentine flow patterns with an active area of 3.5 × 3.5 cm^2 are designed as displayed in Fig. 1a, b, respectively. Each channel was 5 mm wide and 2 mm in depth. The RZAFC assembled with these two flow channel patterns are denoted as "anode-parallel" and "anode-serpentine" cells, respectively. The anode orientations, designated as "anode-top" and "anode-bottom" are shown in Fig. 2a, b, respectively. The investigation of the effect of cell orientation was performed with the parallel flow pattern only.

2.3 Cell performance tests

The cell was first operated by pumping the zinc slurry into the anode flow channel until full. The total weight of zinc powder was approximately 6.0 g. The performance of

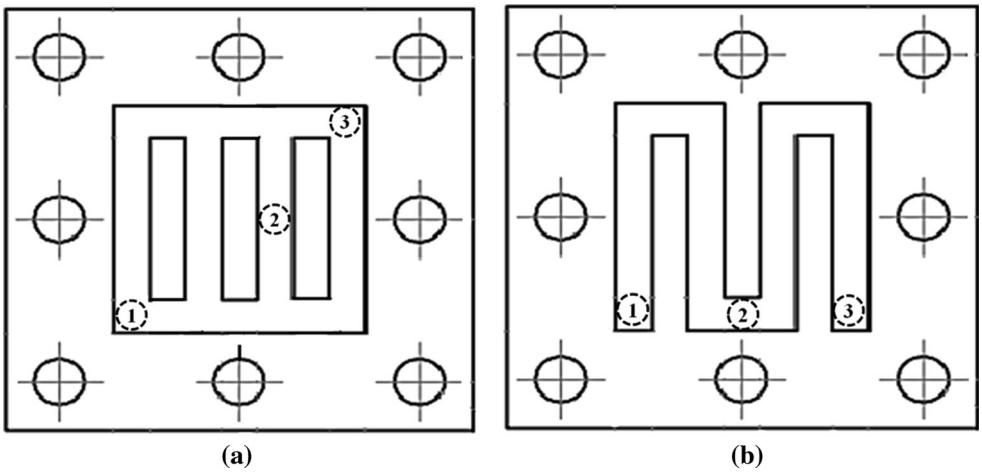

Fig. 1 Anode flow field pattern: **a** parallel and **b** serpentine with the mark number indicating the position in the channel: *1* inlet, *2* midway, and *3* outlet

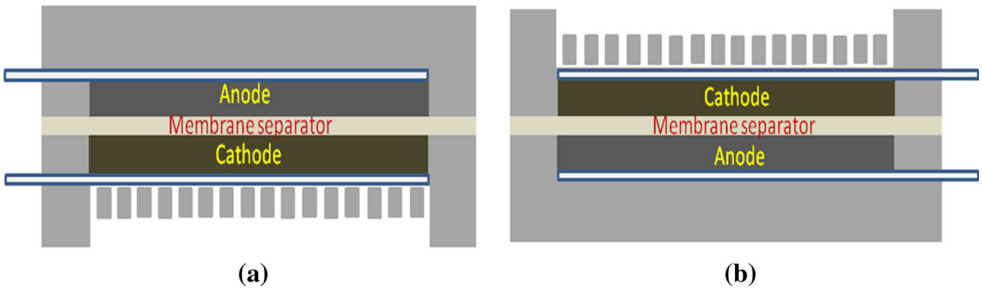

Fig. 2 RZAFC assembly with anode oriented **a** above the cathode (anode-top) and **b** below the cathode (anode-bottom)

RZAFC was tested at room temperature by continuously feeding 8 M KOH electrolyte with a peristaltic pump at one of the flow rates selected (2, 4, and 6 ml h^{-1}). For each flow rate, a new cell was fabricated and tested. At the initial stage of operation, the cell polarization was measured by an electronic load (Agilent Model N3301A) and then evaluated in terms of polarization and power density curves. After that a long-term current discharge test was conducted by drawing a current at a constant voltage of 0.7 V, and the measured results were presented as the chrono-amperometric curves (current density vs. time). The current discharge capacity was evaluated in terms of total charge per gram of zinc by integrating the obtained chrono-amperometric curve and dividing it by the amount of zinc filled in the flow channel.

2.4 Characterization of spent zinc powder

After the long-term current discharge test, the spent zinc powder samples were collected at three different locations along the anode flow channel, as specified in Fig. 1. Then, the samples were characterized for their chemical structure and surface morphology by an X-ray diffractometer (XRD, Bruker: Discover D8) and a scanning electron microscopy (SEM), respectively. A CuKα radiation equipped with a Ni filter was used in the XRD. The tube voltage was maintained at 40 kV with a tube current of 4 mA. The XRD patterns were recorded from 30° to 100° at a scan rate of 0.03° min^{-1}. Moreover, the surface morphology and the XRD pattern of spent zinc samples were compared to that of fresh zinc powder.

3 Results and discussion

3.1 Effect of anode orientation

3.1.1 Cell polarization at the initial stage

The effects of anode orientation in an anode-parallel cell on RZAFC performance were studied with the parallel flow pattern at three different KOH electrolyte flow rates, 2, 4, and 6 ml h^{-1}. First, the polarization characteristic at the initial stage of the operating cell was measured before performing a long-term discharge test, as shown by the polarization and power density curves in Fig. 3. At high electrolyte flow rates of 4 and 6 ml h^{-1}, a better cell performance was obtained from the anode-bottom cell compared to the anode-top cell. However, both cells showed similar performance at the electrolyte flow rate of 2 ml h^{-1}. The maximum power densities of the anode-bottom orientation cell are about 2.4 and 2.0 times higher

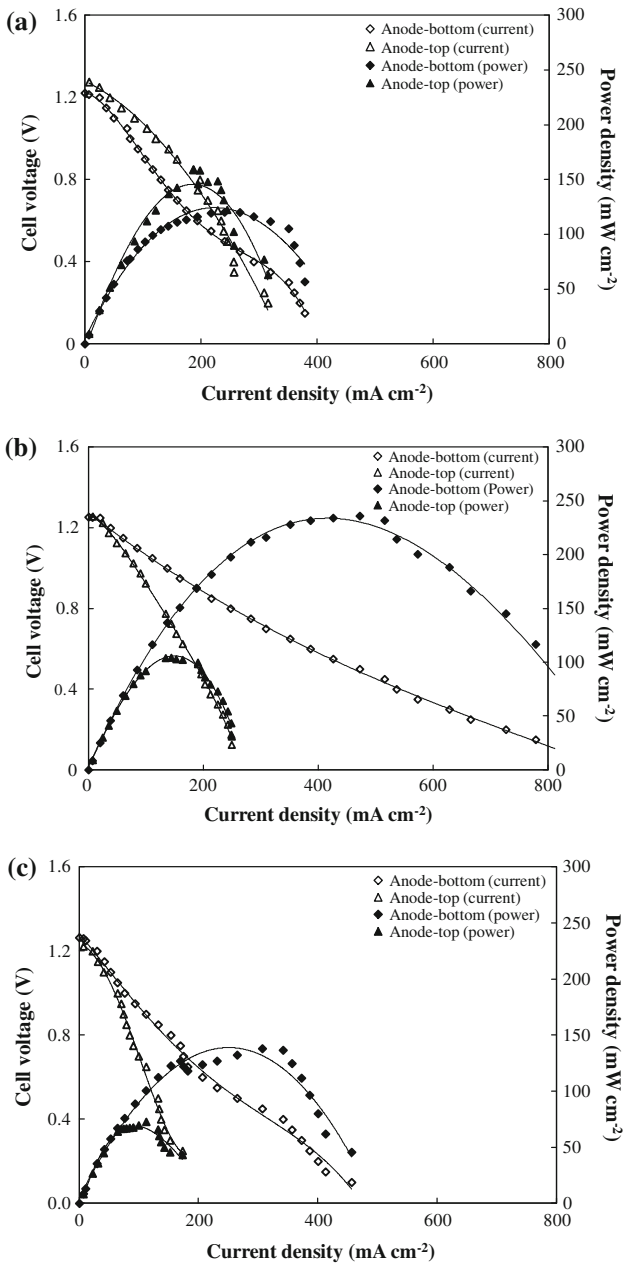

Fig. 3 Polarization and power density curves of anode-top and anode-bottom RZAFCs operated at different electrolyte flow rates: **a** 2, **b** 4, and **c** 6 ml h^{-1}

than that of the anode-top cell at the KOH electrolyte flow rates of 4 and 6 ml h^{-1}, respectively. At a fixed electrolyte flow rate and the same anode configuration, the performance reduction of the anode-top cell should be caused by the cathode polarization loss. For the horizontal orientation, the gravity force acts in the direction perpendicular to the electrode plane. This gravity force induces water to transport across the membrane from the anode to the cathode side, when the anode is arranged above the cathode. The crossover water hindered oxygen diffusion from the atmosphere to the cathode, resulting in the increase of cathode overpotential.

At the electrolyte flow rate of 2 ml h^{-1}, the difference between the maximum power density between the anode-top and the anode-bottom cells became smaller. As shown in Fig. 3b, c, the maximum power densities of the anode-top cell operated at the electrolyte flow rates of 4 and 6 ml h^{-1} were slightly decreased from 100 to 75 mW cm^{-2}. On the other hand, it was tremendously decreased from 240 to 140 mW cm^{-2} for the anode-bottom cell. It could be explained that for the anode-bottom cell, the gravity force acts in the direction from the cathode (top) to the anode (bottom), and hence, could not induce any water transport from the anode up to the cathode. However, it was observed in the experiment of the anode-bottom cell operated at the electrolyte flow rate of 6 ml h^{-1} that there existed a water film on the cathode's surface. As the electrolyte flow rate increased, the pressure inside the anode channel was also enhanced. This pressure drives more water across from the anode to the cathode, causing the performance of the anode-bottom cell to drop and approach closely to that of the anode-top cell.

3.1.2 Long-term current discharge

The effect of anode orientation on the current discharge capacity of RZAFC was investigated by potentiostatic technique, as shown by the chrono-amperometric curves in Fig. 4. The experimental results illustrated that the anode-bottom cell performed better than the anode-top cell for all three electrolyte flow rates. At a low flow rate of KOH electrolyte (2 ml h^{-1}), the current discharge capacity of the anode-bottom cell was slightly better than that of the anode-top cell. However, the difference of current discharge capacity between these two cells became large as the electrolyte flow rate was increased to 4 and 6 ml h^{-1}. The highest current discharge capacity was obtained from the anode-bottom cell operated at the electrolyte flow rate of 4 ml h^{-1}, which corresponded to the polarization curve result shown in Fig. 3. When the electrolyte flow rate was further increased to 6 ml h^{-1}, the current discharge capacity of the anode-bottom cell was still greater than that of the anode-top cell, but the difference between these two cells was less than that in the previous case. The same tendency was also observed in the polarization curve measurement. In addition, the chrono-amperometric curves of the anode-bottom cells had tended to fluctuate more than those of the anode-top cells. This could have been caused by the hydrogen bubble formation inside the parallel anode flow channel as the hydrogen formation rate was enhanced along with the increase of current generated.

For the anode-bottom cell, there was an optimum electrolyte flow rate for obtaining the maximum current

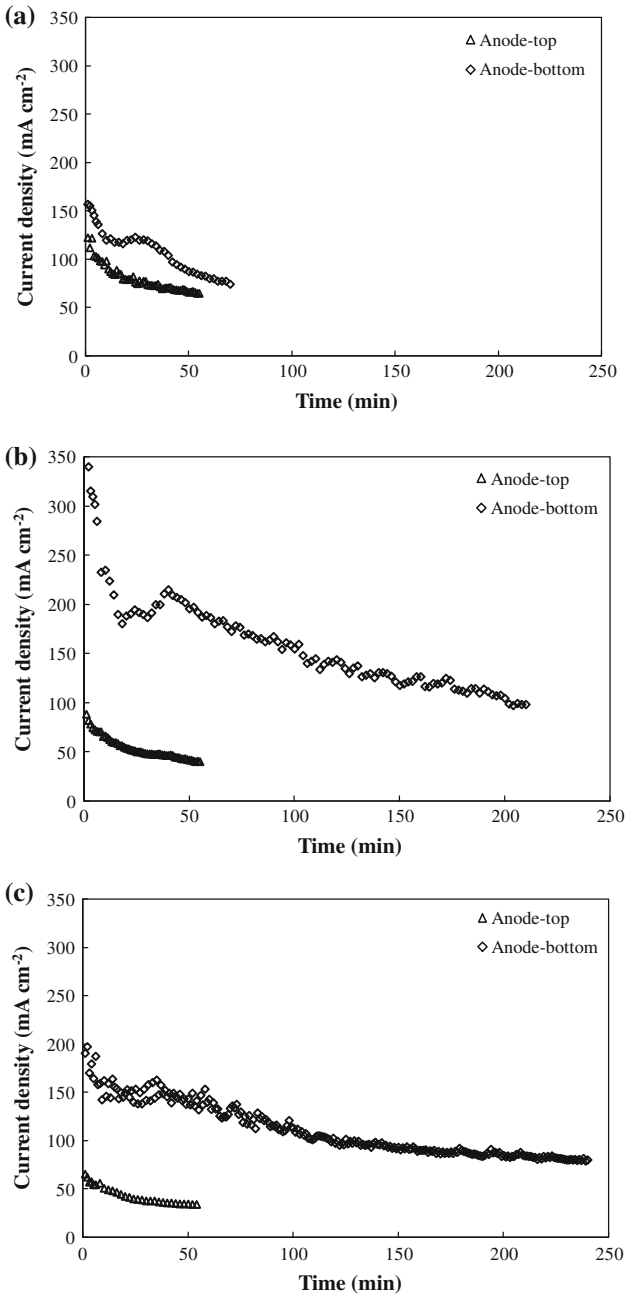

Fig. 4 Long-term discharge curves at a constant 0.7 V of ZAFCs assembled with anode-parallel flow channel for anode-top and anode-bottom cells operating under electrolyte flow rates of **a** 2, **b** 4, and **c** 6 ml h^{-1}

discharge capacity from the cell at 4 ml h^{-1}. A different phenomenon was observed for the anode-top cells. The current discharge capacity of the anode-top cell decreased, when the electrolyte flow rate increased. The starting current density delivered from the cell was 125, 90, and 65 mA cm^{-2} at the electrolyte flow rates of 2, 4, and 6 ml h^{-1}, respectively. As the anode was placed above the cathode, the pressure force exerted by the high flow rate of electrolyte superimposed on gravity drove more water across the membrane, resulting in the more detriment of the cathode performance.

Table 1 Total charge per gram of zinc with different anode orientations using parallel channel under electrolyte flow rates of 2, 4, and 6 ml h^{-1}

KOH flow rate (ml h^{-1})	Total charge per gram of Zn (C g^{-1})	
	Anode-top	Anode-bottom
2	82.39	139.91
4	55.26	627.79
6	43.14	506.63

The anode orientation might have some effects on the anode performance itself if there was an accumulation of H_2 gas produced following Eq (1) and/or (2) inside the cell. According to the direction of gravity force, this H_2 gas would stay at the surface of the membrane for the anode-bottom cell, whereas it preferentially remains inside the flow channel for the anode-top cell. However, the gas accumulation inside the anode was expectedly less due to the drag force exerted by the flowing electrolyte. For a zinc-air fuel cell, the zinc oxidation reaction is faster than the oxygen reduction reaction at the cathode. This is the reason why the cell performance detriment was pointed out to the loss of cathode performance. In addition, for the anode-bottom cell, it was observed that the cell performance was gradually dropped, when the level of anode outlet tube (exit) was raised above the membrane level. The resulted static head drove more water across the membrane leading to a higher flooding at the cathode side.

The total charges generated per gram of zinc reactant for all cases were calculated by integrating the chronoamperometric curves to obtain the area under the curves and then dividing them by the amount of zinc powder loaded in the anode flow channel. The calculated total charges per gram of zinc obtained from both the anode-bottom and the anode-top cells are summarized in Table 1. It was found that the total charge per gram of zinc generated from the anode-top cell decreased with the increase of the electrolyte flow rate, whereas the total charge per gram of zinc obtained from the anode-bottom cell was maximum at the electrolyte flow rate of 4 ml h^{-1}. The zinc utilization of the anode-bottom cell was about 11.4 times that of the anode-top one at this electrolyte flow rate. For the anode-bottom cell, further increase in the electrolyte flow rate from 4 to 6 ml h^{-1} had decreased the total charge per gram of zinc by approximately 20 %. Actually, the concentration of OH^- ions was high throughout the flow channel, when the electrolyte flow rate was high. Thus, the anode performance of zinc-air fuel cells should be enhanced according to the anode oxidation reaction as follows [1]:

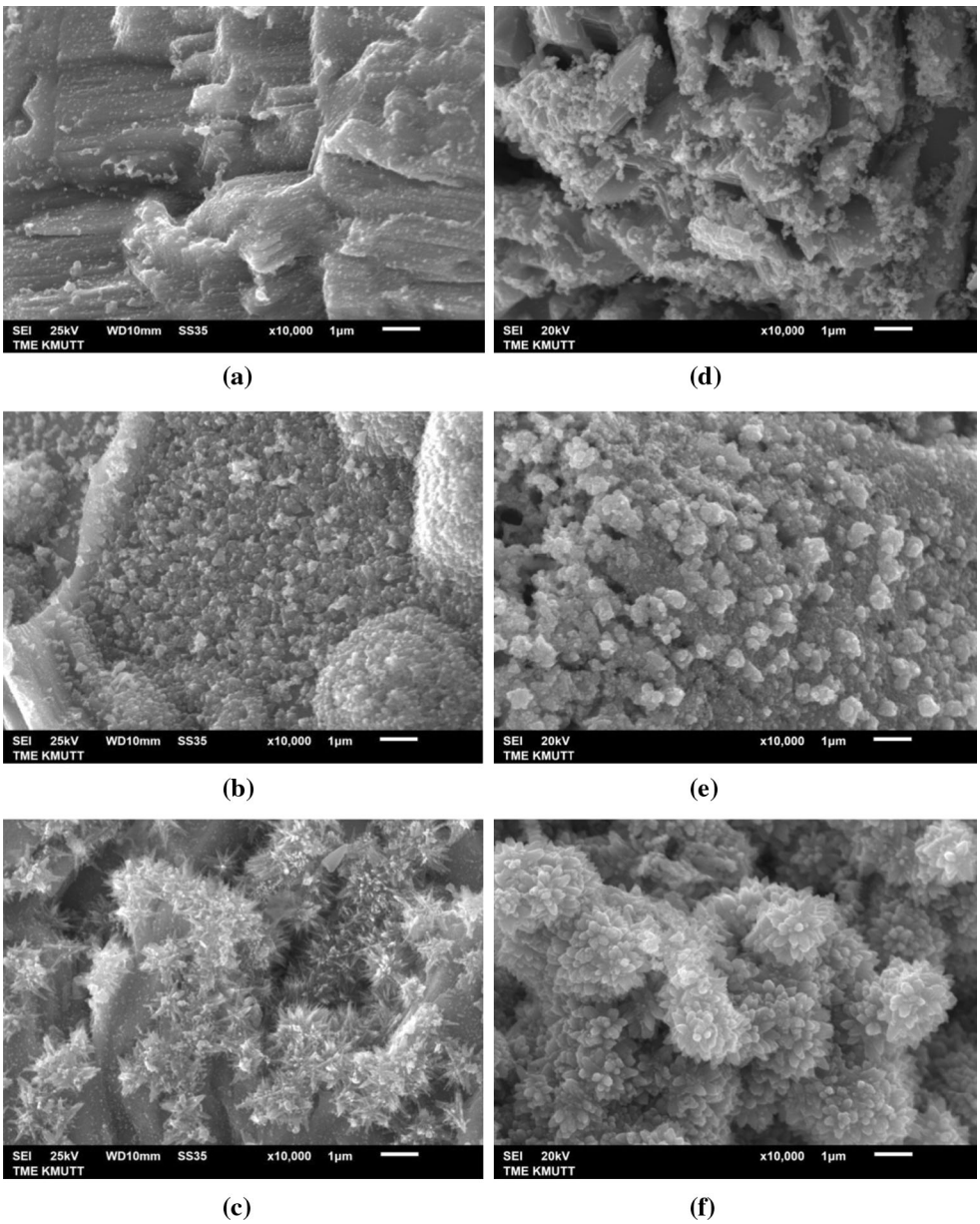

Fig. 5 SEM images of spent zinc samples collected from three locations of anode-parallel channel in anode-top cell: **a** inlet, **b** mid-way, and **c** outlet; and in anode-bottom cell: **d** inlet, **e** mid-way, and **f** outlet. The cell was operated at 2 ml h^{-1} electrolyte flow rate

$$Zn \rightarrow Zn^{2+} + 2e^{-} \quad (3)$$

$$Zn^{2+} + 4OH^{-} \rightarrow Zn(OH)_4^{2-} \quad (4)$$

$$Zn(OH)_4^{2-} \rightarrow ZnO + H_2O + 2\ OH^{-} \quad (5)$$

Therefore, the performance reduction of the anode-top cell should be caused by the cathode over-potential.

3.1.3 Characterization of the spent zinc powder

As displayed in Figs. 5, 6 and 7, the SEM images present the surface morphology of the utilized zinc powder after the long-term discharge test. Three samples were taken at the inlet, the mid-way and the outlet of the flow field in order to reveal the reaction situation occurring at each electrolyte flow rate. As previously found by many researchers [13, 14], the fresh zinc surface presents a smooth surface, whereas needle-like and spongy-like structures have been proven to be a ZnO phase. The ZnO phase on the sample taken from the anode-bottom cell appeared more than that from the anode-top cell at the same electrolyte flow rate, confirming higher zinc utilization by the former orientation.

One important difference between the SEM images of the zinc powder used by the two anode orientations was

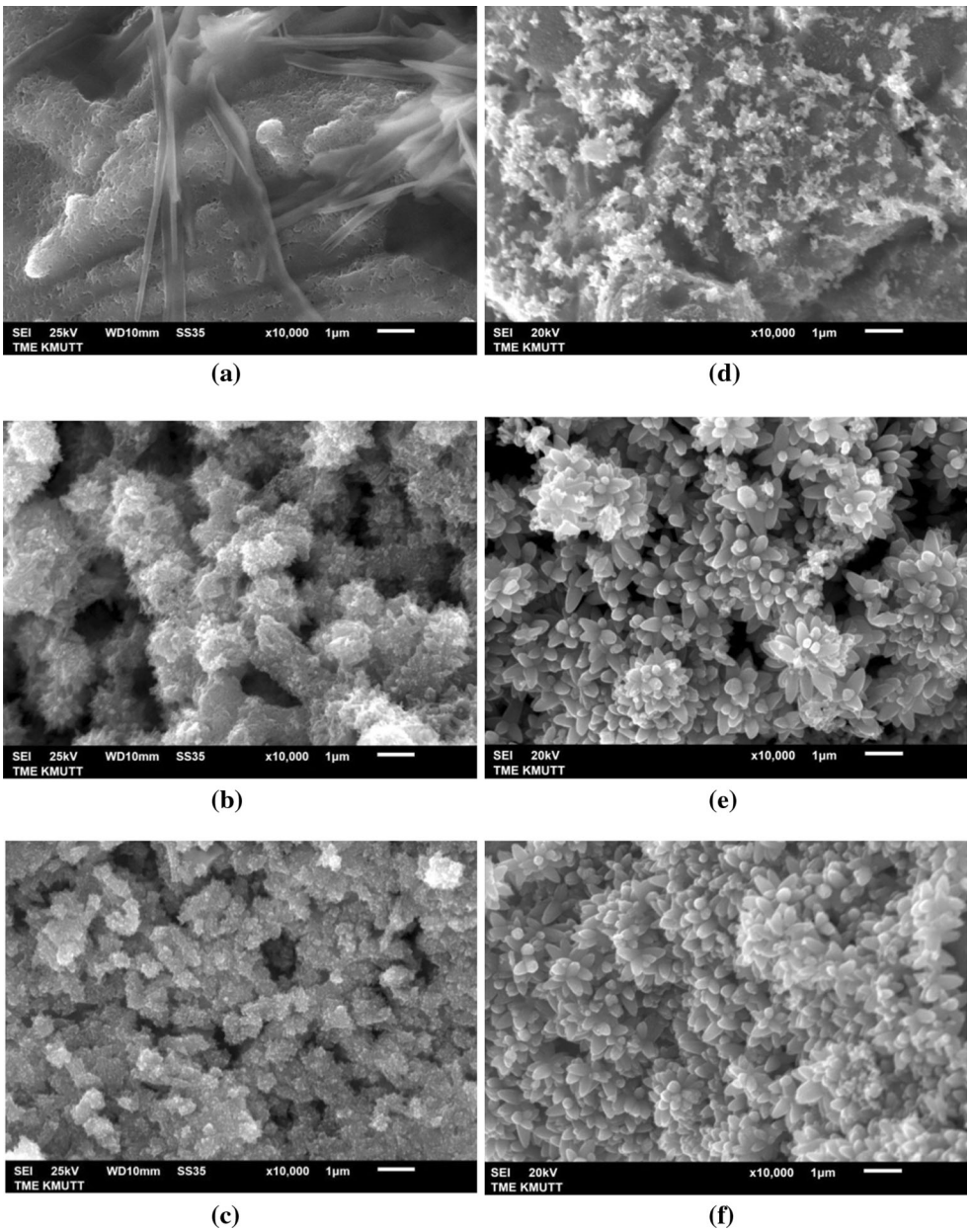

Fig. 6 SEM images of spent zinc samples collected from three locations of anode-parallel channel in anode-top cell: **a** inlet, **b** mid-way, and **c** outlet; and in anode-bottom cell: **d** inlet, **e** mid-way, and **f** outlet. The cell was operated at 4 ml h^{-1} electrolyte flow rate

that the ZnO phase in the spent zinc sample collected from the anode-bottom cell had aggressively grown from the inlet to the outlet, whereas a non-uniform growth along the flow channel length in the samples was observed in the anode-top cell. Nevertheless, one similarity among the samples taken from both orientations at all three electrolyte flow rates was that there were fewer white precipitates on the surface of the samples taken from the inlet location. This supports the concept of the anode reactions as presented in Eqs. (3)–(5). Initially, the zinc metal is oxidized to release electrons and form zinc (II) ions. This process will proceed until the solubility of the zincate ions, $Zn(OH)_4^{2-}$ (aq), reaches a saturation point. After exceeding this point, zincate ions further react and form ZnO phase. For the flowing electrolyte, the zincate ions had been continuously carried along the channel, yielding low concentrations of these ions at the inlet region. As a result, the possibility of forming ZnO at this location was less. As the KOH electrolyte flowed along the channel, concentrations of these ions continually increased, which then enhanced the chance of ZnO formation at the mid-way and the outlet locations of the channel.

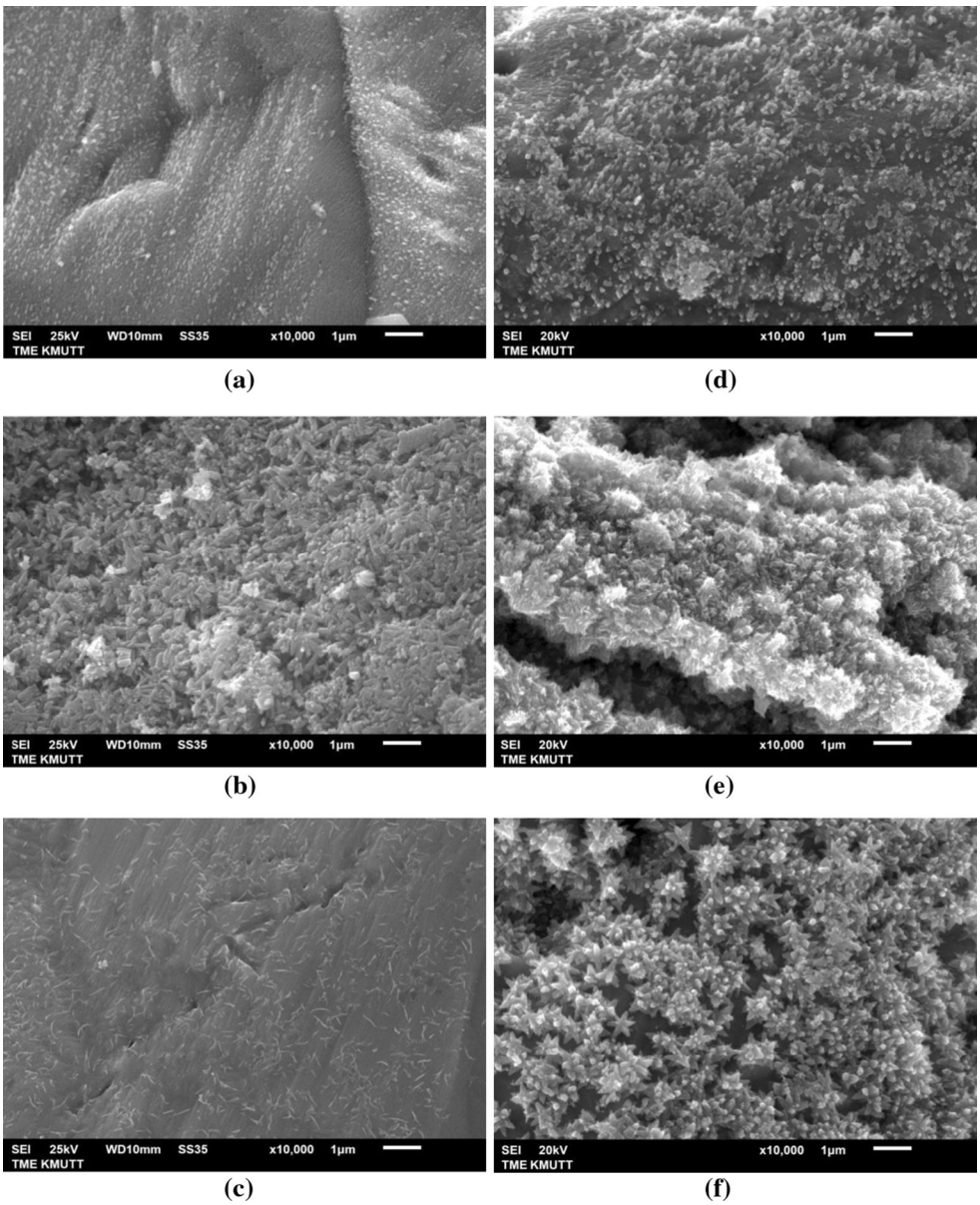

Fig. 7 SEM images of spent zinc samples collected from three locations of anode-parallel channel in anode-top cell: (**a** inlet, **b** mid-way, and **c** outlet; and in anode-bottom cell: **d** inlet, **e** mid-way, and **f** outlet. The cell was operated at 6 ml h^{-1} electrolyte flow rate

In addition, the needle-like structure on the zinc sample taken from the anode-bottom cell at the electrolyte flow rate of 6 ml h^{-1} was quite loose compared to the case of the electrolyte flow rate of 4 ml h^{-1}, even though the difference between the current discharge capacities of both cases was only 20 % (See Figs. 6 and 7). This is because the concentration of zincate ions inside the cell was decreasing as the electrolyte flow rate increased. Moreover, zincate ions left the anode flow channel too early to form the ZnO phase when the cell was operated at an overly high electrolyte flow rate.

The XRD patterns of the spent zinc samples taken from the anode-top cells were compared to those of fresh zinc and from the anode-bottom cells, as depicted in Fig. 8. The fresh zinc displayed characteristic peaks of Zn metal at 2θ of 36.31°, 39.01°, 43.20°, 54.35°, 70.66°, 82.09°, and 89.85°. As compared to the pattern of fresh zinc, the peak intensities of the Zn metal of all the spent zinc samples had been diminished, especially the peaks at 2θ of 36.31°, 39.01°, as observed in the case of the anode-bottom cell. The maximum reduction of the Zn metal peak intensity was observed for the case of the anode-bottom cell with the electrolyte flow rates of 4 and 6 ml h^{-1}, which is consistent with the long-term discharge results, indicating the highest utilization of Zn.

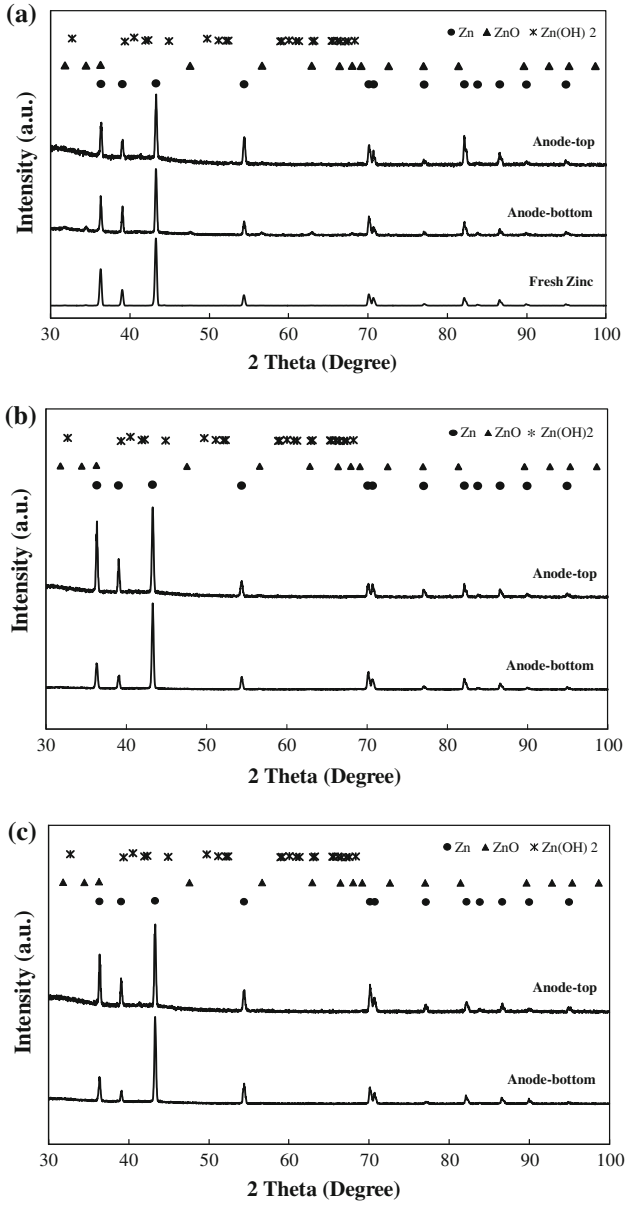

Fig. 8 XRD patterns of spent zinc anode powder collected from anode-top and anode-bottom cells operated at different electrolyte flow rates: **a** 2, **b** 4, and **c** 6 ml h^{-1}

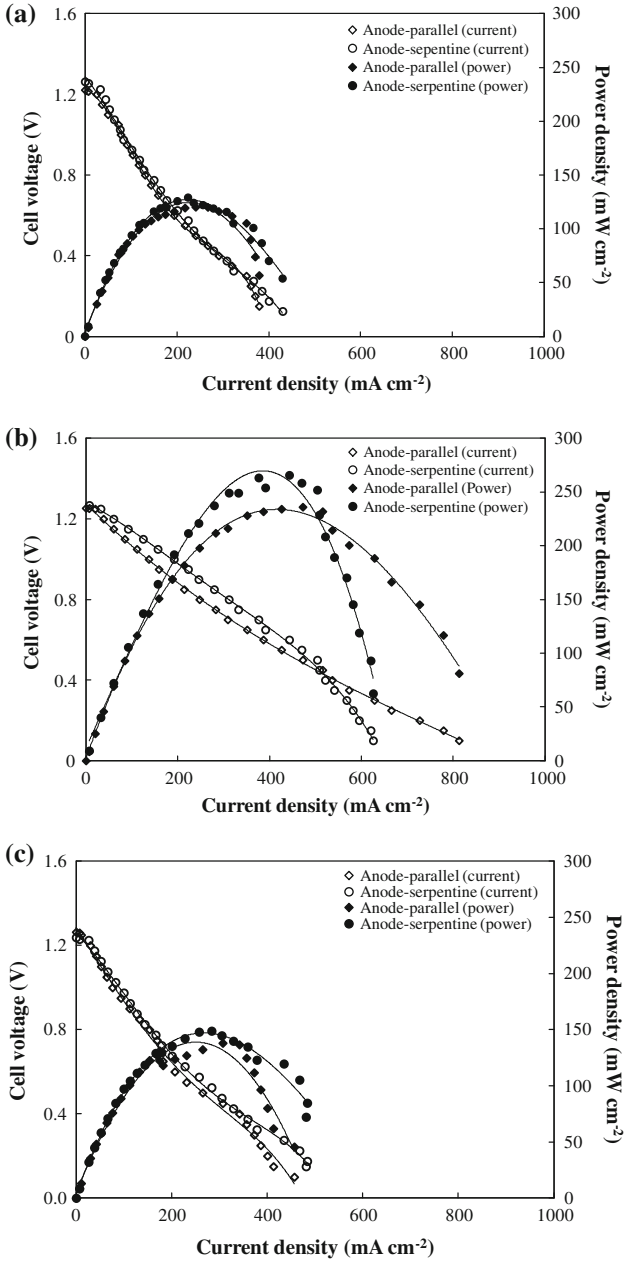

Fig. 9 Polarization and power density curves of anode-bottom RZAFC having different anode channel designs operated at different electrolyte flow rates: **a** 2 ml h^{-1}, **b** 4 ml h^{-1}, and **c** 6 ml h^{-1}

3.2 Effect of anode flow channel design

3.2.1 Cell polarization at the initial stage

According to the above results, the effects of anode flow channel design with parallel or serpentine patterns were investigated with the anode-bottom cell due to the better performance of this orientation. Moreover, it was found that there was an optimum electrolyte flow rate for the anode-parallel flow channel pattern. Therefore, the influence of the electrolyte flow rate on the performance of the anode-serpentine flow channel was also tested at different values of 2, 4, and 6 ml h^{-1}. The performance curves at the initial stage of cell operation for both flow channel patterns at three electrolyte flow rates are compared in Fig. 9. The performance of the anode-serpentine cell was close to that of the anode-parallel cell at every electrolyte flow rate. The influence of the electrolyte flow rate on the serpentine flow field performance showed a similar trend as found in the parallel flow field. The

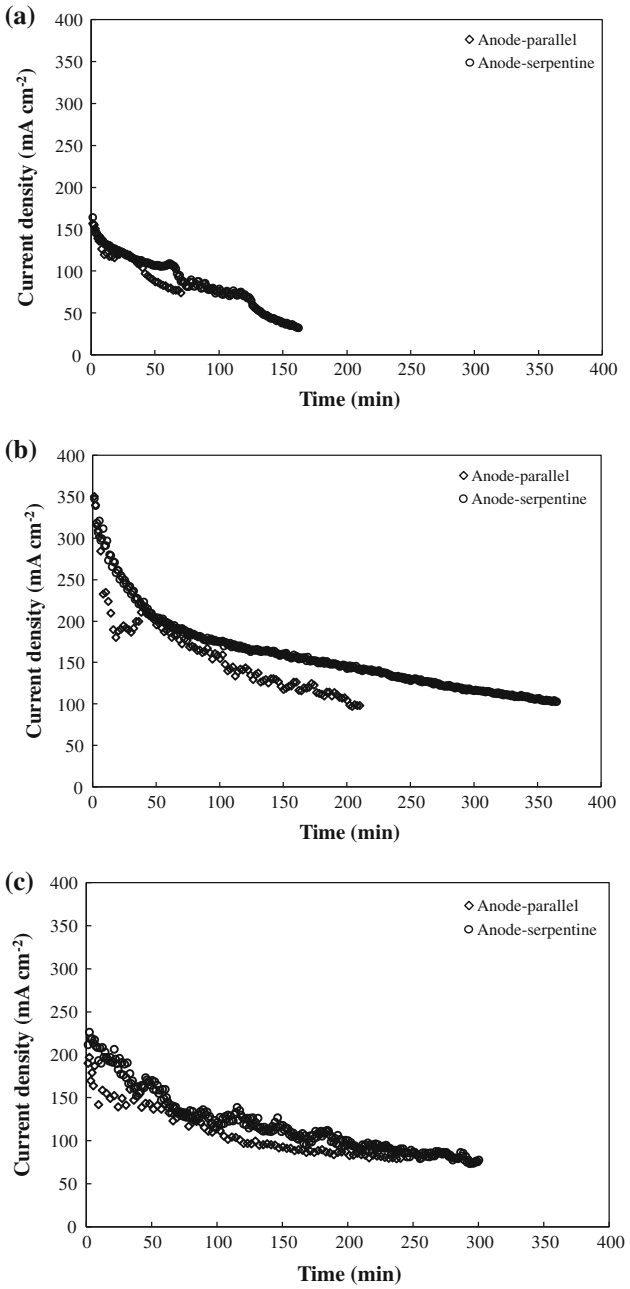

Fig. 10 Long-term discharging curves at 0.7 V of anode-bottom RZAFC having serpentine and parallel flow channels and operating at different electrolyte flow rates of **a** 2 ml h^{-1}, **b** 4 ml h^{-1} , and **c** 6 ml h^{-1}

optimum flow rate of electrolyte for the anode-serpentine cell was at 4 ml h^{-1}, which was the same as that of the anode-parallel cell. At a low flow rate of electrolyte (2 ml h^{-1}), the maximum power densities of both cells were around 125 mW cm^{-2}. As the electrolyte flow rate increased to 4 ml h^{-1}, the anode performance was improved, and the maximum power density of the anode-parallel and the anode-serpentine cells was increased to 240 and 270 mW cm^{-2}, respectively. However, further increase of the electrolyte flow rate to 6 ml h^{-1} inversely reduced the maximum power density of both cells to about 140 mW cm^{-2}. The augmentation of the pressure inside both anode flow fields with the increase of electrolyte flow rate forced more water crossover from anode to cathode, resulting in high cathode polarization as previously discussed.

Table 2 Total charge per gram of zinc with different anode flow channel patterns and % excess KOH under electrolyte flow rates of 2, 4, and 6 ml h^{-1}

KOH electrolyte flow rate (ml h^{-1})	Total charge per gram Zn (C g^{-1})		% excess KOH	
	Anode-parallel	Anode-serpentine	Anode-parallel	Anode-serpentine
2	139.91	267.15	116	158
4	627.79	1,106.94	186	180
6	506.63	687.52	549	458

3.2.2 *Long-term current discharge*

Figure 10 shows the long-term discharge curves of the anode-serpentine and the anode-parallel cells at three electrolyte flow rates of 2, 4, and 6 ml h^{-1}. At the electrolyte flow rates of 2 and 6 ml h^{-1}, both anode-serpentine and anode-parallel cells displayed similar performance. However, at the optimum electrolyte flow rate of 4 ml h^{-1}, the anode-serpentine cell performed much better than the anode-parallel cell. At this value, the current density discharged at 0.7 V of both anode-serpentine and anode-parallel cells started almost at the same value ($\sim$350 mA cm^{-2}), but the current delivered from anode-parallel cell dropped much faster than that from the anode-serpentine cell. Consequently, the discharge time of the anode-serpentine cell was much longer than that of the anode-parallel cell.

The total charge per gram of zinc calculated by the same procedure as previously mentioned for the anode-serpentine cell is also included in Table 2. The maximum charge per gram of Zn was obtained from the anode-serpentine cell at the electrolyte flow rate of 4 ml h^{-1}. At this electrolyte flow rate, the total charge per gram of zinc delivered from the anode-serpentine cell was 1.75 times that of the anode-parallel one. It should be mentioned that the total charge per gram of zinc obtained from the anode-serpentine cell was higher than that from the anode-parallel cell for every electrolyte flow rate.

It should also be mentioned that all the electrolyte flow rates selected to study could provide excess KOH amount for the anode oxidation reaction. From the area under the chrono-amperometric curves, the total charge produced was calculated and the total amount of KOH required for the reaction could be obtained. The excess amount of KOH

for the three flow rates was in the range of 116-549 % depending on the types of flow field as summarized in Table 2.

One important phenomenon observed from the chrono-amperometric curves was the fluctuation of the discharged current in time. It is surmised that this fluctuation had been caused by H_2 bubble formation inside the cell. When H_2 gas accumulated inside the cell, a three-phase region among solid (zinc), liquid (KOH electrolyte), and gas (H_2) existed. As the H_2 gas surrounded the zinc powders, the discharged current lessened, since these bubbles inhibit OH^- ions to access the unreacted zinc surface. As the H_2 bubbles were detached from the zinc surface by the shear force acted from the flowing electrolyte, the discharged current heightened again. This cycling process was repeated during discharge time.

At a low electrolyte flow rate of 2 ml h^{-1}, both anode-serpentine and anode-parallel cells exhibited fluctuations in the current. If the electrolyte flow rate is too low, the shear force exerted by the electrolyte is insufficient to expel the hydrogen gas from the anode flow field. One might expect that the fluctuation of the chrono-amperometric curve should be the highest at the lowest flow rate of electrolyte. However, the fluctuation depended not only on the amount of H_2 gas that had been pushed out from the cell, but also the amount of H_2 gas generated inside the cell. The higher the electrolyte flow rate, the larger the quantity of H_2 gas that was generated.

The chrono-amperometric curve of the anode-parallel cell still fluctuated even at high electrolyte flow rates. The fluctuation of current discharged from the anode-parallel cell at the electrolyte flow rate of 4 ml h^{-1} was quite large, especially at the early stage of discharge time. For the first 20 min of discharge time, the current discharged from the anode-parallel cell was abruptly dropped. Then, the current slightly increased during the 20–40 min of the discharge time. After 40 min, the current generated from this cell gradually declined with small fluctuations of current density. On the other hand, the anode-serpentine cell discharged current very smoothly, especially at this optimum flow rate. It can be inferred that the serpentine flow field had expelled H_2 gas more effectively than had the parallel flow field. In the serpentine flow field, the electrolyte had been forced into a single flow channel leading to a higher fluid velocity, and consequently, higher shear force. In contrast, the electrolyte in the parallel flow field was able to move through many pathways, resulting in a lower fluid velocity, and thus, lowering the shear force. As a result, the chance of H_2 gas accumulation inside the parallel flow field was higher than that in the serpentine flow field. The superior performance of the serpentine flow field to the parallel flow field was also discovered in direct methanol fuel cells. Under test conditions in the parallel flow field, the CO_2 bubbles blocked the flow channel, whereas this phenomenon was not observed in the serpentine flow field [10].

As the flow rate of electrolyte increased to 6 ml h^{-1}, the discharged current at the initial stage of the anode-parallel cell began at 200 mA cm^{-2} and proceeded with small magnitudes of fluctuation. The current density discharged from the cell steadily decreased as the fluctuation decreased. Although H_2 gas was being continuously removed from the cell as the flow rate of electrolyte increased, H_2 gas generation also increased with the electrolyte flow rate. Therefore, the fluctuation existed in both flow fields at the electrolyte flow rate of 6 ml h^{-1}, but the sudden drop of the current density at the initial stage of the discharge time as found in the case of 4 ml h^{-1} still appeared in the anode-parallel cell.

3.2.3 *Characterization of the spent zinc*

The SEM images showing surface morphology of the spent zinc powders collected from the anode-serpentine cell operated under different electrolyte flow rates (2, 4, and 6 ml h^{-1}) are displayed in Fig. 11. The images on the top (Fig. 11a, d, g), the middle (Fig. 11b, e, h), and the bottom rows (Fig. 11c, f, i) belong to the samples taken from the inlet, the mid-way, and the outlet of the anode-serpentine cell, respectively. These figures indicate that for all the electrolyte flow rates, the needle-like structure of the ZnO phase had grown out of the inlet through to the outlet. At the inlet location, the size of the structure on the zinc surface operated at the lowest electrolyte flow rate (2 ml h^{-1}) was the largest of the three flow rates. By comparing the SEM images of the spent zinc samples between the anode-serpentine and the anode-parallel cells at the same location and with the same electrolyte flow rate, one can observe that the sizes of the needle-like structures on the spent zinc taken from the anode-serpentine cells were generally smaller than those from the anode-parallel cell. The higher shear force occurring inside the serpentine flow field prevented the growth of the needle-like structure. Particularly, at the electrolyte flow rate of 6 ml h^{-1}, there was no significant growth of this structure along the flow channel and the smooth surface of the unreacted zinc was clearly visible. The zincate ions were swept out of the cell by the flowing electrolyte before decomposing into the ZnO phase on the zinc surface.

At the electrolyte flow rate of 4 ml h^{-1} providing the best performance of both anode-serpentine and anode-parallel cells, the aggressive growth of the needle-like structure was observed on the zinc surface of both cells, but their morphologies were different. The shape of the needles on the sample collected from the anode-serpentine cell was much longer and sharper than the one from the anode-

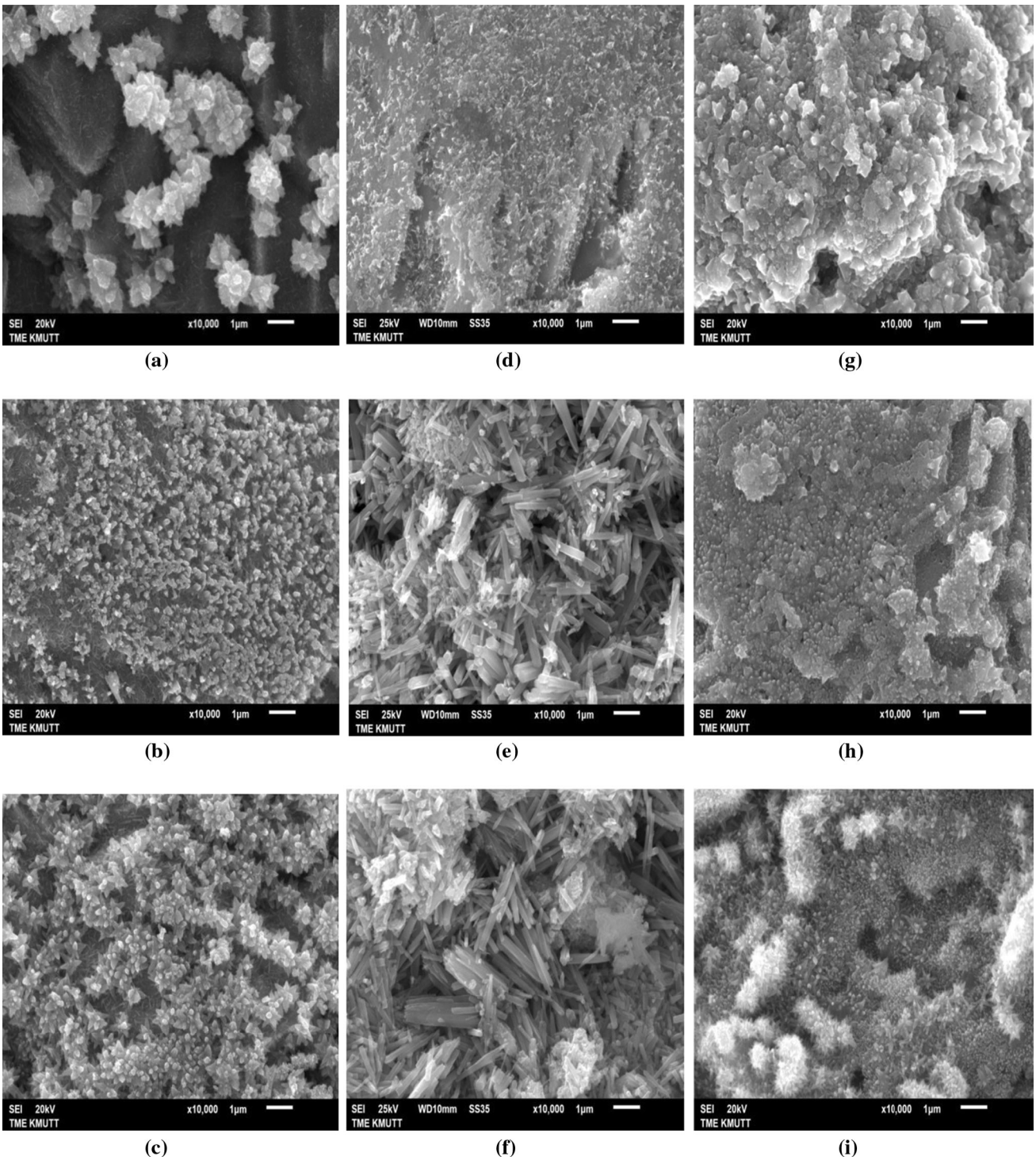

Fig. 11 SEM images of spent zinc samples collected at three locations of anode-serpentine channel of the anode-bottom cell: row **a**, **d**, **g** for inlet, row **b**, **e**, **h** for mid-way, and **c**, **f**, **i** for outlet, operated at different electrolyte flow rates: column **a**, **b**, **c** for 2 ml h^{-1}, **d**, **e**, **f** for 4 ml h^{-1}, and **g**, **h**, **i** for 6 ml h^{-1}

parallel cell. In addition, the manner of the deposition of the needle on both samples was different. Most needle-like particles on the zinc powder samples taken from the parallel flow channel attached firmly to the solid surface, whereas the needle-like particles on the zinc collected from the serpentine flow channel seemed to detach from the solid surface and loosely pack together. In fact, the shape of the ZnO phase on the spent zinc powder taken from the

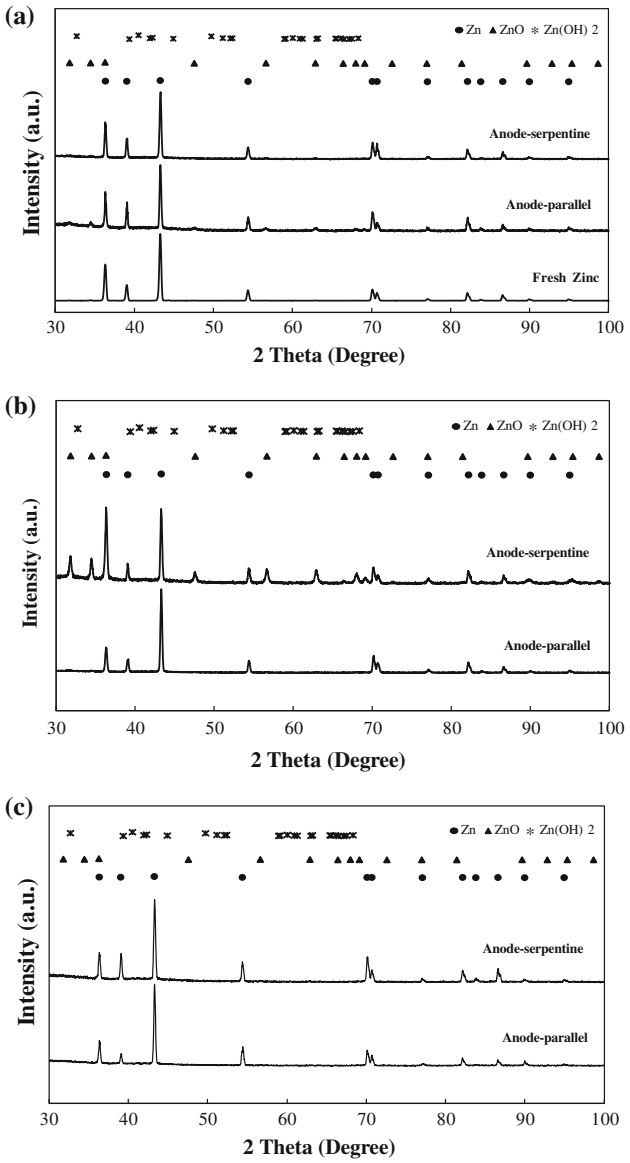

Fig. 12 XRD patterns of spent zinc anode powder collected from anode-top and anode-bottom cells operated at different electrolyte flow rates: **a** 2 ml h^{-1}, **b** 4 ml h^{-1}, and **c** 6 ml h^{-1}

anode-serpentine cell looked more like a rod than a needle. This morphology might have contributed to the highest current discharge capacity of the anode-serpentine cell at the electrolyte flow rate of 4 ml h^{-1}. The detached needle-like particles might have been caused by a higher shear force in the serpentine flow field.

Figure 12 shows the XRD patterns of the spent zinc powder between the anode-serpentine and the anode-parallel cells. The characteristic peaks of the ZnO phase at 2θ of 47.53°, 56.60°, 62.86°, and 67.90° were clearly observed in the sample taken from the anode-serpentine cell at the electrolyte flow rate of 4 ml h^{-1}. These characteristic peaks belong to ZnO(102), ZnO(103), Zn(112), and ZnO(201), respectively [13]. The XRD results confirmed that the maximum zinc utilization had taken place in the anode-serpentine cell at the electrolyte flow rate of 4 ml h^{-1}. In addition, the characteristic peaks of zinc hydroxide, $Zn(OH)_2$, at 2θ of 31.77° and 34.42° appeared in both the serpentine and the parallel flow channels. The appearance of the $Zn(OH)_2$ phase ensured the formation of hydrogen gas inside the cell because this phase involves the H_2 evolution reaction according to Eqs. (1)–(2).

4 Conclusion

In this study, the effects of anode orientations and anode flow field designs on the performance of ZAFC were investigated at three KOH electrolyte flow rates of, 2, 4, and 6 ml h^{-1}. First, the effect of anode orientation with the parallel flow pattern was studied. The orientation of the anode below the cathode produced higher maximum power density for the cell at the initial stage of operation than did the orientation above the cathode, especially at the optimum electrolyte flow rate of 4 ml h^{-1}. In addition, the current discharge capacity of the anode-bottom cell operating at this optimum flow rate was 11.4 times higher than that of the anode-top cell. The cell performance of the anode-top cell was lower because of the existence of a water film on the cathode surface, resulting in high cathode mass transport overpotential. The water film had resulted from water crossover from the anode to the cathode which was induced by the gravity force. Furthermore, more aggressive growth of the needle-like particles of the ZnO along the flow channel was found in the spent zinc taken from the anode-bottom orientation cell, whereas nonuniform growth of the ZnO phase was observed in the sample collected from three locations of the cell with anode-top orientation.

Secondly, the effect of the anode flow channel design on the RZAFC's performance was conducted with the anode-bottom orientation cell. At the initial stage of operation, the cell performance curve of the anode-serpentine cell was similar to that of the anode-parallel one. The highest maximum power density of both cells was obtained at the electrolyte flow rate of 4 ml h^{-1}. However, at this optimum electrolyte flow rate, the long-term current discharge from the anode-parallel cell dropped faster than that from the anode-serpentine cell. The total charge per gram of zinc delivered from the anode-parallel cell was about 0.57 times that from the anode-serpentine one. At high electrolyte flow rates (either 4 or 6 ml h^{-1}), the higher shear force occurring inside the serpentine flow field prevented the growth of the needle-like particles of the ZnO phase inside the cell and expelled the H_2 out of the cell more effectively than did the parallel flow field.

Acknowledgments The authors would like to acknowledge the financial support of the National Research Council of Thailand (NRCT), and the Higher Education Research Promotion and National Research University (NRU) Project of Thailand, Office of the Higher Education Commission, and the Department of Chemical Engineering, King Mongkut's University of Technology Thonburi (KMUTT).

References

1. Lee JS, Kim ST, Cao R, Choi NS, Liu M, Lee KT, Cho J (2011) Metal-air batteries with high energy density: Li-Air versus Zn-Air. Adv Energy Mater 1:34–50
2. Zhang XG (2006) Fibrous zinc anodes for high power batteries. J Power Sources 163:591–597
3. Stuart I, Smedley X, Zhang G (2007) A regenerative zinc-air fuel cell. J Power Sources 165:897–904
4. Goldstein J, Brown I, Koretz B (1999) New developments in the electric fuel Ltd. zinc/air system. J Power Sources 80:171–179
5. Neburchilov V, Wang H, Martin JJ, Qu W (2010) A review on air cathodes for zinc-air fuel cells. J Power Sources 195:1271–1291
6. Pei P, Ma Z, Wang K, Wang X, Song M, Xu H (2014) High performance zinc air fuel cell stack. J Power Source 249:13–20
7. Sapkota P, Kim H (2009) Zinc-air fuel cell: a potential candidate for alternative energy. J Ind Eng Chem 15:445–450
8. Jiricny V, Siu S, Roy A, Evans JW (2000) Regeneration of zinc particles for zinc-air fuel cells in a spouted-bed electrode. J Appl Electrochem 30:647–656
9. Hayre O, Cha SW, Colella W, Prinz FB (2009) Fuel cell fundamentals, 2nd edn. Wiley, Hoboken
10. Yang H, Zhao TS, Ye Q (2005) In situ visualization study of CO_2 gas bubble behaviour in DMFC anode flow fields. J Power Sources 139:79–90
11. Oliveira VB, Rangel CM, Pinto AMFR (2010) Effect of anode and cathode flow field design on the performance of a direct methanol fuel cell. Chem Eng J 157:174–180
12. Szczesniak B, Cyrankowska M, Nowacki A (1998) Corrosion kinetics of battery zinc alloys in electrolyte solution. J Power Sources 75:130–138
13. Yap CK, Tan WC, Alias SS, Mohamad AA (2009) Synthesis of zinc oxide by zinc-air system. J. Alloys Compd 484:934–938
14. Cho YD, Fey GTK (2008) Surface treatment of zinc anodes to improve discharge capacity and suppress hydrogen gas evolution. J Power Sources 184:610–616